Thesis for the degree of Licentiate of Engineering

A New Audiometric Bone Vibrator, Radioear B81, and the Bone Conduction Implant with Emphasis on Magnetic Resonance Imaging

by

Karl-Johan Fredén Jansson

Department of Signals and Systems
Biomedical Signals and Systems Group
CHALMERS UNIVERSITY OF TECHNOLOGY

Göteborg, Sweden 2015

A New Audiometric Bone Vibrator, Radioear B81, and the Bone Conduction Implant with Emphasis on Magnetic Resonance Imaging

Karl-Johan Fredén Jansson

This thesis has been prepared using LaTeX.

Licenciatavhandlingar vid Chalmers Tekniska Högskola
Ny serie nr R0002/2015.
ISSN 1403-266X

Department of Signals and Systems
Biomedical Signals and Systems Group
Chalmers University of Technology
SE-412 96 Göteborg, Sweden

tel: +46 31 772 1000
fax: +46 31 772 1783
email: karljohf@chalmers.se

Printed by Chalmers Reproservice
Göteborg, Sweden 2015

Till Sofia, Mamma, Pappa, Johannes, Samuel, Mormor & Morfar

A New Audiometric Bone Vibrator, Radioear B81, and the Bone Conduction Implant with Emphasis on Magnetic Resonance Imaging

Karl-Johan Fredén Jansson
Department of Signals and Systems
Biomedical Signals and Systems Group
Chalmers University of Technology

Abstract

Hearing by air conduction (AC) and bone conduction (BC) are attributed to be the natural ways of stimulating the cochlea. With AC hearing, the cochlea is stimulated by air pressure variations via the ear canal, whereas with BC hearing, sound vibrations are transmitted thru the skull bone to the cochlea. Sensorineural hearing losses are commonly rehabilitated with conventional AC hearing aids in the ear canal, but patients who are suffering from conductive or mixed hearing losses, and who are unable to use AC hearing aids, may instead use bone conduction devices (BCDs). In order to determine the type and degree of hearing loss, the BC hearing thresholds are measured using a bone vibrator, and then analyzed together with the AC hearing thresholds to suggest an appropriate rehabilitation alternative.

This thesis deals with two BC hearing related topics. The first topic is evaluating a new audiometric bone vibrator, Radioear B81, which is assumed to offer more accurate BC hearing threshold measurements. The second topic is related to a new type of active transcutaneous BCD, called the Bone Conduction Implant (BCI), which leaves the skin intact by using a wireless solution that does not require a permanent skin penetration. Even though the applications are different, both devices use the same Balanced Electromagnetic Separation Transducer (BEST) principle as motor unit in their design.

The audiometric bone vibrator Radioear B81 was found to have an improved low frequency performance and can produce higher output levels with less harmonic distortion than was possible before. In a clinical study of the first six patients, it was found that the BCI is a realistic alternative to already commercially available BCDs. In technical evaluations, the BCI was shown to be insensitive to skin thickness variations and to have robust output, and that it possibly tolerates magnetic resonance imaging at 1.5 Tesla.

Keywords: balanced electromagnetic separation transducer, bone conduction, bone vibrator, retention magnet, image artifact, demagnetization, magnetically induced torque, magnetic resonance imaging.

Acknowledgments

Acknowledgments

First of all, I would like to thank professor Bo Håkansson for inspiring me to become a researcher and for all the interesting projects and thank you for all your support. Thank you Sabine Reinfeldt for your supervision and support with writing. Thank you Hamidreza Taghavi for your invaluable support with images and LaTeX. Thank you Cristina Rigato for all your support with writing and measurements. Thank you Måns Eeg-Olofsson for all your great support with writing and the surgeries of the BCI patients. Thank you Tomas Tengstrand and Leif Johannsen for your help and support with the Radioear B81 studies, and thanks to Ortofon A/S for the bone vibrator samples. Thanks to family, friends and relatives who are always there for me and special thanks to my love Sofia for making everything so much easier, and I would like to thank her family for their encouragement and support.

List of papers

This thesis is based on the following papers.

I Electro-Acoustic Performance of the New Bone Vibrator Radioear B81: A comparison with the conventinal Radioear B71. Fredén Jansson, K-J., Håkansson, B., Johannsen, L. and Tengstrand, T. *International Journal of Audiology*, Published ahead of print, 2014.

II MRI Induced Torque and Demagnetization in Retention Magnets for a Bone Conduction Implant. Fredén Jansson, K-J., Håkansson, B., Reinfeldt, S., Taghavi, H. and Eeg-Olofsson, M. *IEEE Transactions on Biomedical Engineering,* 2014; 61(6):1887-1893.

III MRI Investigation of the Bone Conduction Implant - a pilot study at 1.5 Tesla. Fredén Jansson, K-J., Rigato, C., Håkansson, B., Reinfeldt, S. and Eeg-Olofsson, M. In Manuscript, 2015.

IV Technical Design of a New Bone Conduction Implant (BCI) System. Taghavi, H., Håkansson, B., Reinfeldt, S., Eeg-Olofsson, M., Fredén Jansson, K-J., Håkansson, E. and Nasri, B. Accepted after minor revision *International Journal of Audiology*, 2015. This is a revised version of Paper VI in the PhD thesis of Hamidreza Taghavi 2014, ISBN 978-91-7385-970-7.

V The Bone Conduction Implant - Clinical results of the first six patients. Reinfeldt, S., Håkansson, B., Taghavi, H., Fredén Jansson, K-J. and Eeg-Olofsson, M. *International Journal of Audiology*, Published ahead of print, 2015.

Other publications by the author, not included in the thesis:

- The Bone Conduction Implant - First Implantation, Surgical and Audiologic Aspects. Eeg-Olofsson, M., Håkansson, B., Reinfeldt, S., Taghavi, H., Lund, H., Fredén Jansson, K-J., Håkansson, E. and Stalfors, J. *Otology & Neurotology* 2014; 35(4):679-685.

- Evaluation of Bone Tissue Formation in a Flat Surface Attachment of a Bone Conduction Implant - A pilot study in a sheep model. Eeg-Olofsson M., Johansson C.B., Lith A., Håkansson B., Reinfeldt S., Taghavi H., and Fredén-Jansson, K.J. *Audiology & Neurotology Extra* 2014; 4(3):62-76.

Please note
Parts of Paper I have been presented as follows:

- Fredén Jansson, K-J., Håkansson, B., Johannsen, L. and Tengstrand, T. (2013). "A New Audiometric Bone Conductor - B81 for more accurate hearing results," S2 Workshop, Chalmers University of Technology, Department of Signals and Systems, Göteborg, Sweden.

- Fredén Jansson, K-J. (2014). "The Electro-Acoustic Performance of the New Bone Vibrator Radioear B81 - a comparison with the conventional Radioear B71", AudiologyNOW! 2014 Experience the Magic - AAA, Florida, Orlando, USA.

- Fredén Jansson, K-J., and Taghavi, H. (2014). "Nya Audiometriska Benledaren Radioear B81 - en elektroakustiskt jämförelse med Radioear B71," Svensk Teknisk Audiologisk Förening (STAF), Halmstad, Sweden.

- Fredén Jansson, K-J. (2014). "Electro-Acoustic Performance of the New Bone Vibrator Radioear B81 - a comparison with the conventional Radioear B71," Medicinteknikdagarna, Göteborg, Sweden.

Parts of Papers II and III have been presented as follows:

- Fredén Jansson, K-J., Håkansson, B., Reinfeldt, S., Taghavi, H. and Eeg-Olofsson, M. (2013). "MRI induced torque and demagnetization in retention magnets for Bone Conduction Implants," 4^{th} International Symposium on Bone Conduction Hearing - Craniofacial Osseointegration, Newcastle, UK.

- Fredén Jansson, K-J., and Taghavi, H. (2014). "MRI Induced Torque and Demagnetization in Retention Magnets for Bone Conduction Implants," Svensk Teknisk Audiologisk Förening (STAF), Halmstad, Sweden.
- Fredén Jansson, K-J. (2014). "MRI Induced Torque and Demagnetization in Retention Magnets for a Bone Conduction Implant," ISMRM/SMRT Workshop on Safety in MRI: Guidelines, Rationale & Challenges, Washington, DC, USA.
- Fredén Jansson, K-J. (2014). "MRI Induced Torque and Demagnetization in Retention Magnets for a Bone Conduction Implant," Medicinteknikdagarna, Göteborg, Sweden.

Contents

Abbreviations and Acronyms

AC	Air Conduction
AM	Amplitude Modulation
AP	Audio Processor
APHAB	Abbreviated Profile of Hearing Aid Benefit
ASTM	American Society for Testing Materials
BAHA	Bone Anchored Hearing Aid
BEST	Balanced Electromagnetic Separation Transducer
BC	Bone Conduction
BCD	Bone Conduction Device
BCI	Bone Conduction Implant
dB	Decibel
dB HL	Decibel Hearing Level
GBI	Glasgow Benefit Inventory
GE	Gradient-Echo
MR	Magnetic Resonance
MRI	Magnetic Resonance Imaging
PA	Power Amplifier
RF	Radio Frequency
SE	Spin-Echo
SPL	Sound Pressure Level
SSD	Single Sided Deafness
THD	Total Harmonic Distortion
VSB	Vibrant Soundbridge

Part I

Introductory chapters

Chapter 1

Introduction

Hearing by air conduction (AC) and bone conduction (BC) are attributed to the natural ways of stimulating the cochlea. In BC hearing, the cochlea is stimulated via sound vibrations in the skull bone, whereas in AC hearing, which is considered to be the normal way of hearing, it is stimulated via air pressure variations in the ear canal. Diagnostic hearing investigations of patients with suspected hearing loss comprises both AC and BC hearing threshold testing. In the BC threshold testing, sound vibrations are induced in the skull bone by a bone vibrator placed on the forehead or the mastoid part of the temporal bone behind the ear to assess the degree of sensorineural hearing loss. Rehabilitation of sensorineural hearing loss is most commonly done by using conventional AC hearing aids with a speaker worn in the opening of the ear canal. The difference between the AC and BC thresholds determines the so called air-bone gap, which is commonly interpreted as a so called conductive hearing loss. If a patient has both an air-bone gap greater than zero and a sensorineural hearing loss, the patient is said to suffer from a mixed hearing loss. Patients with conductive or mixed hearing loss are more likely to benefit from rehabilitation using a bone conduction device (BCD), which stimulates the cochlea by converting AC sound into mechanical vibrations in the skull bone.

In recent years, the trend has led towards the development of new semi or fully implantable BCDs that offer new benefits for patients. However, these devices have also introduced some new challenges. One challenge is to more accurately diagnose the patient in order to suggest the best possible rehabilitation alternative. Another challenge is to safely perform magnetic resonance imaging (MRI) in patients with implantable BCDs. One example of such a new implantable BCD is the Bone Conduction Implant (BCI), developed at Chalmers University of Technology and Sahlgrenska University

Hospital, both located in Göteborg, Sweden. For the BCI, there is a great interest to investigate how the MRI interacts with magnetic and electric conductive materials, both from a diagnostic and patient safety perspective.

This thesis deals with two topics related to BC hearing. The first topic is presenting a new bone vibrator called Radioear B81 (Radioear Corporation, Pennsylvania, USA), which is a device that generates a BC sound during measurements of sensorineural hearing loss. The second topic is related to a hearing implant, the BCI, with an emphasis on issues regarding MRI of such a device. Both devices use the same balanced electromagnetic separation transducer (BEST) principle as motor unit to create vibrations in the skull bone, which is comprehensively described in Chapter 3.1.4. The BEST principle was invented and explored by Håkansson (2003) to improve the poor low frequency performance of conventional transducers and to offer a more efficient, lighter and smaller design that is suitable for implantation. Generally speaking, the BEST principle is a balancing technique that improves linearity so that distortion is reduced. In a collaboration between Chalmers University of Technology and Ortofon A/S in Denmark, the BEST design was further developed and optimized for efficient serial production to be used as the motor unit in the new audiometric bone vibrator B81. Up till now, the most frequently used bone vibrator is the Radioear B71 (Radioear Corporation, Pennsylvania, USA) which was developed in the 1970′s. Unfortunately, the B71 has some well-known limitations at low frequencies, but since it is the most widely used bone vibrator, the B81 has been designed to replicate the frequency response shape and electrical characteristics of the B71 in order to be compatible with the same type of audiometers. The B71 has been updated with some minor changes over the years, but has always used the conventional variable reluctance type transducer principle. Recently, a new version was released under the trade name B71W and is a modified version of B71 to comply with the RoHS directive 2011/65/EU (Radioear, 2015a).

The BEST transducer in the BCI is much smaller than in the B81 and has other frequency characteristics in order to be more suitable for implantation and hearing rehabilitation. It is implanted in a 4-5 mm deep recess drilled in the mastoid part of the temporal bone to give an osseointegrated and direct bone drive with no soft tissues in-between. A wireless link supplies the transducer with a sound signal from an audio processor that is magnetically attached over the skin to the patient′s head. By leaving the skin intact, the risks for skin complications, such as those from skin penetrating implants, are eliminated. In an ongoing clinical study approved by the Swedish Medical Agency and the regional Ethical Review Board, the BCI shows significant hearing rehabilitation of patients with conductive or mild-to-moderate mixed hearing loss. Furthermore, studies of the MRI safety of the BCI have been

conducted and the results show that the present design is likely to pass a conditional approval to be scanned in a 1.5 Tesla MRI scanner.

1.1 Aim of thesis

The overall aim of this thesis is to present two new devices used in the field of bone conduction hearing; the bone vibrator Radioear B81 and the BCI system. In Paper I, the aim was to evaluate the electro-acoustic performance of the Radioear B81 in comparison with the conventional Radioear B71.

In the papers related to the BCI system (Paper II-V), the general aim was to investigate its safety and effectiveness as a transcutaneous BCD for rehabilitation of patients with conductive or mild-to-moderate mixed hearing loss. In detail, the aim with Paper II and III was to investigate effects and risks related to the use of a the BCI in MRI, such as magnetically induced torque, demagnetization, image artifacts, induced sound and performance. In Paper IV, the technical design of the BCI system is presented with the aim to describe and technically verify its performance in terms of current consumption, retention force and output characteristics. The aim of Paper V was to present the audiological and patient related outcomes for the first six patients implanted with the BCI by summarizing their audiometric results and measures from two validated questionnaires at the 6-month follow up visit.

1.2 Thesis outline

Followed by the introductory Chapter 1, where the objective and problem descriptions are presented, Chapter 2 describes basic hearing physiology and bone conduction audiometry as well as gives the principles of MRI. An overview of the devices investigated in this thesis is given in Chapter 3. Appended papers (I-V) are shortly summarized in Chapter 4 and their most important outcomes are concluded in Chapter 5 together with plans for future studies.

Chapter 2

Basics of audiology and magnetic resonance imaging

2.1 Audiology - a brief overview

The natural function of the human ear is to transform airborne sound to nerve signals that are transmitted to higher centres in the brain. This transformation can be explained by dividing the ear into three components: the outer ear, the middle ear and the inner ear. An illustration of the ear anatomy is given in Figure 2.1. The outer ear is where airborne sound enters the ear and consists of the pinna and ear canal. In the interface between the outer and middle ear, the tympanic membrane (eardrum) is located, which moves accordingly to air-pressure variations in the ear canal. The middle ear is a cavity of air, comprising the ossicular chain which transmits the motions of the tympanic membrane to the oval window, which is the entrance window to the cochlea (inner ear). These vibrations are transformed into a travelling wave in the cochlear fluids causing hair cells on the basilar membrane to generate electrical response signals that are transmitted via the auditory nerve and further to the brain for sound interpretation.

The cochlea can also be stimulated directly from vibrations in the skull bone, for example from a person′s own voice when speaking, or from a transducer that vibrates the bone. Hearing through the ear canal and vibrations in the bone are attributed to air conduction (AC) and bone conduction (BC) hearing, respectively. In Figure 2.2, the AC and BC pathways are illustrated, both from a vibrating transducer and from a person′s own voice.

Disorders of the outer, middle or inner ear will cause different types of hearing losses. Those are conductive hearing loss, sensorineural hearing loss (SNHL) or both. Patients who are suffering from conductive hearing loss

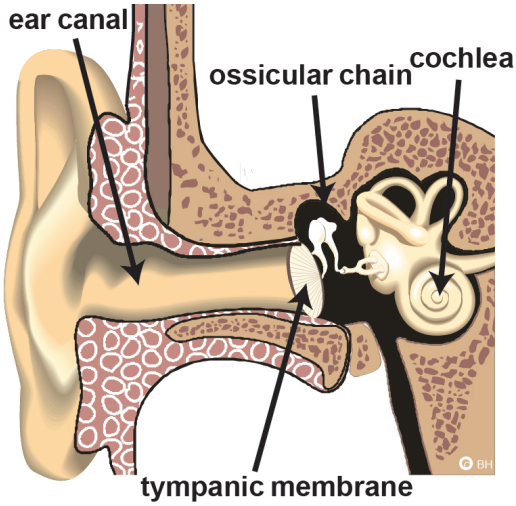

Figure 2.1: The anatomy of the human ear showing the ear canal, tympanic membrane, ossicular chain and the cochlea.

have a malfunction in the outer and/or the middle ear, while SNHL typically refers to an impairment of the inner ear or the auditory nerve pathway to the brain. A patient who is completely deaf has no sensorineural hearing. Complete deafness on one ear is called single sided deafness (SSD).

2.2 Audiometry and rehabilitation

A patient′s hearing is documented and illustrated in a graphic representation called audiogram, comprising both AC and BC hearing thresholds for left and right ear and, if needed, with masking. The hearing thresholds are measured using an audiometer that creates sounds at different hearing levels and frequencies for both AC and BC testing. If AC hearing is tested, the sound is applied by headphones and, if BC hearing is tested, it is applied with a bone vibrator. The headphones incorporates two small speakers, one for each ear, whereas the bone vibrator is pressed towards the skin with a steel spring on the forehead or, or more commonly, on the mastoid part of the temporal bone behind the pinna of the ear.

The BC thresholds are compared with normal hearing levels to reveal the degree of SNHL, while a conductive hearing loss is found by calculating the so called air-bone gap, which is the difference between the AC and BC thresholds. There are many possible causes of SNHL, but it is commonly related to aging and exposure to high sounds that have damaged the hair cells in the inner ear. There are also different classifications of SNHL de-

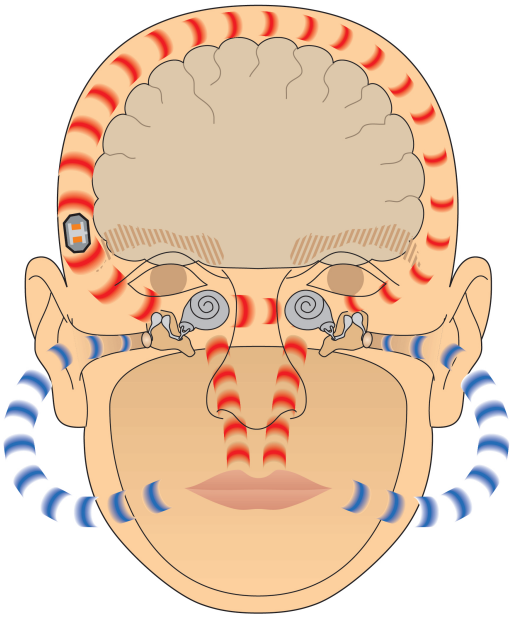

Figure 2.2: An illustration of the air conduction (blue) and bone conduction (red) pathways of the sound from a person′s own voice and an implanted transducer in the temporal bone.

pending on its severity which varies from slightly (16-25 dB HL) to profound (>90 dB HL). Patients with conductive hearing loss are less frequent than patients with SNHL and have other possible causes, such as chronic ear infections, earwax and other problems associated with the outer and middle ear (Clark, 1981). Depending on the severity and type of hearing loss, there are different types of devices for hearing rehabilitation. Patients with SNHL are commonly rehabilitated with conventional AC hearing aids that amplify the sound directly in the ear canal, but in severe cases, SNHL patients are rehabilitated with cochlear implants.

Conductive hearing loss is different from SNHL in the sense that the outer and/or middle ear obstructs the sound from reaching the inner ear. Patients who are suffering from conductive hearing loss or who are unable to use conventional AC hearings aids are commonly rehabilitated with a bone conduction device (BCD). These devices stimulates the cochlea by creating vibrations in the skull bone. Sometimes, BCDs are also used to provide rehabilitation for patients with mixed hearing loss or SSD. When using a BCD, the airborne sound is transformed by an audio processor (AP) to electric signals that drive a vibrating transducer, giving vibrations that are bypassing the obstructed outer and middle ear. The position of the transducer and

invasiveness of the device will depend on the type of BCD. Conventional BCDs are non-invasive and work similar to bone vibrators with the transducer pressed against the skin over the skull bone with a static force, except that they are battery driven and transform airborne sound into vibrations. A more invasive BCD is the percutaneous bone anchored hearing aid (BAHA) with a skin-penetrating abutment anchored to the bone by the use of a titanium fixture. Passive and active transcutaneous BCDs use an implanted unit under the skin and are thereby skin-intact solutions (Reinfeldt et al., 2015). As the trend during recent years has been to develop fully-or-semi implantable hearing devices, new materials have been introduced in the body that raise new questions regarding safety issues. The focus in this thesis is on active transcutaneous BCDs and in particular the bone conduction implant (BCI) developed in Göteborg, Sweden, with emphasis on aspects concerning magnetic resonance imaging (MRI).

2.3 Safety aspects of magnetic resonance imaging

MRI is used as a diagnostic tool to visualize internal structures of the human body by letting soft tissue and fluids interact with magnetic fields (Bushong, 2003). A patient that is using an implantable medical device should not undergo an MRI examination if it has not been proven to be safe (Shellock, 2012). The reason for this is that the magnetic fields from the MRI scanner interact with implants made of magnetic or electric conductive materials, which is the case for hearing implants, pacemakers and some prosthetic implants. There are mainly three components of the magnetic fields of the MRI scanner: the static field, the radio frequency (RF) field and the gradient field.

Permanent magnets and ferromagnetic materials tend to align with the static field, which induces forces and torque that cause risks, such as implant damage and dislocation, and in the worst case, injures the patient (Teissl et al., 1998). The RF and gradient fields are time-varying fields that can induce electrical currents in electric conductive materials, such as conductive wires and loops, but they can also induce eddy currents in metal plates and some magnetic materials. Some risks with induced currents are heat generation, damaging of electronic components and implant stimulation (Nyenhuis et al., 2005; McComb et al., 2009). The American Standard for Testing Materials (ASTM) has developed guidelines and recommendations on how to evaluate the MRI safety risks regarding implants. After testing, the implant can be labeled either as MR safe, MR unsafe or MR conditional. The latter

label is the most common for implantable BCDs and means that scanning is only allowed under certain conditions (Shellock, 2012).

Today, the only commercial available active transcutaneous BCD is Bonebridge™ (MED-EL Corp., Innsbruck, Austria), which is approved as MR conditional at 1.5 Tesla. The commercially available passive transcutaneous BCDs are Sophono™ Alpha 2 (Sophono Inc., Denver, USA), MR conditional at 1.5 and 3 Tesla, and the Baha® 4 Attract (Cochlear Ltd., Sydney, Australia), MR conditional at 1.5 Tesla.

The Vibrant Soundbridge (VSB) from MED-EL is an active transcutaneous middle ear implant with the transducer attached to the long process of the incus (Jesacher et al., 2010; Beltrame et al., 2009). Compared to BCDs, the transducer vibrates the ossicular chain instead of the skull bone and stimulates the cochlea via the oval window. The MRI safety of the VSB has been thoroughly investigated, but has not until recently been approved as MR conditional at 1.5 Tesla (MED-EL, 2014).

2.3.1 The static magnetic field

Soft tissue and fluids inside the human body consists of hydrogen, which has gyromagnetic properties. The purpose of the static field is to magnetize the human body in one direction by aligning hydrogen protons in a gyroscopic rhythm with precision, referred to as equilibrium. This will make the aligned protons rotate with a deflection angle around the equilibrium direction in a gyroscopic motion. The amount of aligned magnetization M and the frequency of rotation will depend on the magnetic flux density B_0 of the static magnetic field of the MRI scanner, which is given in the unit Tesla. The rotation frequency is commonly referred to as the Larmor frequency f_L and is calculated as

$$f_L = \frac{\gamma}{2\pi} B_0, \tag{2.1}$$

where $\gamma/2\pi$ is the gyromagnetic constant, which is 42.6 MHz/Tesla for hydrogen (Bushong, 2003). This means that f_L is approximately 64 and 128 MHz for a 1.5 and 3 Tesla MRI scanner, respectively. According to Boltzmann′s distribution (Haacke et al., 1999), the stronger the static magnetic field is, the stronger will the magnetization signal for a proton density ρ be at temperature T according to

$$M = \frac{\rho \gamma^2 h^2}{16\pi^2 k_b T} B_0, \tag{2.2}$$

which is an advantage in terms of resolution, acquisition time and signal to noise ratio. However, a higher B_0 requires that the RF coils can work at higher frequencies and most importantly, the magnetically induced torque

Γ on implants that contain magnetic materials will increase. The magnetic torque can be approximated as,

$$\Gamma = mB_0 sin\theta, \tag{2.3}$$

where θ is the angle between the direction of the static magnetic field of the MRI scanner and the magnetic moment m of the implant (Coey, 2010; Todt et al., 2011).

2.3.2 The radio frequency field

Once the body is magnetized in the direction of the static magnetic field, the RF field is applied to manipulate the magnetization. The RF field is a sequence of RF pulses with the Larmor frequency to excite the gyroscopic motion of the magnetization. This will cause the deflection angle to increase and make the magnetization deviate from equilibrium and then fall back again. The time it takes for the magnetization to fall back to equilibrium is called the relaxation time and varies for different types of tissues with different hydrogen densities. Different types of pulse sequence are used for scanning with specific pulse combinations in time, direction and, together with gradient fields, at specific locations. The RF field is applied and measured simultaneously using different coil types, specially designed for scanning of the whole body, knee or head (Bushong, 2003).

2.3.3 The gradient field

The gradient field is used to excite the magnetization at different locations in the body by creating a gradient in the static magnetic field. This changes the Larmor frequency over the body except in the location where the excitation is desired. By switching the gradient for different locations, response signals can be distinguished from different locations in the body and collected as data for image reconstruction. The switched gradient fields should not be confused with the spatial gradient field, which is static and caused by the uniform field inside the bore as it decays around the scanner (Shellock et al., 2011).

Chapter 3

Devices

3.1 Bone vibrators

Diagnostic hearing investigations of patients with suspected hearing loss comprises both AC and BC threshold testing. A bone vibrator is the device that applies the sound when BC hearing thresholds are measured for the assessment of SNHL. It is attached to the skin on the forehead, or more commonly, on the mastoid part of the temporal bone, using a steel spring, and it is driven by a calibrated audiometer to generate hearing levels at different frequencies.

3.1.1 Radioear B71

The B71 from Radioear (Radioear Corporation, Pennsylvania, USA) has been the most widely used bone vibrator since the 1970′s (Gallichan et al., 1998) and is shown in Figure 3.1. Recently, Radioear released the B71W, which has practically identical performance as B71, but does not contain any lead in order to comply with the RoHS directive 2001/65/EU (Radioear, 2015a). Examples of other bone vibrators developed over the years are, from Radioear, the B70 and B72, and from Grahnert Präcitronic GmbH, Germany, the KH70. The Radioear devices are characterized by their three distinct and damped resonance peaks, while the KH70 only has one low frequency peak, but a flatter and smoother frequency response at higher frequencies (Richards and Frank, 1982). Furthermore, the KH70 radiates less airborne sound, but is large and heavy, which makes it hard to attach behind the ear without touching the pinna (Håkansson, 2003; Stenfelt and Goode, 2005). However, even though the B71 is the standard bone vibrator, it has some well-known limitations in its performance at low frequencies where it generates a large amount of non-linear distortion at higher hearing levels. Over the years, this

Figure 3.1: External view of the Radioear B71.

has led to the fact that BC hearing thresholds are rarely tested below 500 Hz using the B71 because of the inherent second order distortion of variable reluctance type transducers. A comprehensive description of the variable reluctance type transducer is given in Håkansson (2003) and is summarized below.

3.1.2 The variable reluctance type transducer

The variable reluctance type transducer in the Radioear B71 is electromechanically transmitting vibrations to its housing when it is driven by a time-varying current, *i(t)*. This current flows through a pair of twin coils that are winded around two yoke arms to create a time-varying flux, $\Phi_{\sim}$, in an air-gap, see Figure 3.2. A permanent magnet with a static magnetic flux, Φ_0, is positioned between the twin coils to achieve a static force in the air-gap that is maintained using a counteracting suspension spring. As long as $\Phi_{\sim}$ varies within $\pm\Phi_0$, the air-gap will open and close accordingly to $\Phi_{\sim}$ and the total vibrating force, F_{tot}, of the transducer will be proportional to ($\propto$) the total magnetic flux in the air-gap squared so that

$$F_{tot} \propto (\Phi_0 + \Phi_{\sim})^2 = \Phi_0^2 + 2\Phi_0\Phi_{\sim} + \Phi_{\sim}^2, \tag{3.1}$$

where it can be seen that F_{tot} is nonlinearly depending on $\Phi_{\sim}$. For small values of $\Phi_{\sim}$, where the nonlinear effect is negligible, $2\Phi_0\Phi_{\sim}$ is much greater than $\Phi_{\sim}^2$. For higher values of $\Phi_{\sim}$, harmonic distortion is generated, especially at low frequencies, which causes an accuracy problem in BC audiometry. In order to minimize this nonlinear effect, a permanent magnet with a high static magnetic flux is needed to achieve a higher static force in the air-gap. This will require a stiffer suspension spring to maintain the air-gap, but a stiffer spring will move the lower resonance peak to a higher frequency. Unfortunately, a relatively low resonance frequency is required in BC audiometry

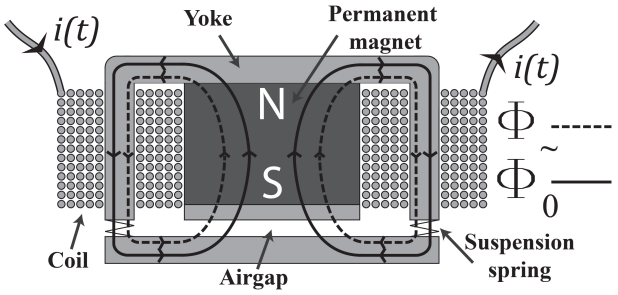

Figure 3.2: Cross-sectional view of the variable reluctance transducer in the B71 bone vibrator.

and can only be regained by increasing the counteracting mass, m, making the bone vibrator heavier. One such example is the Radioear B72, which is a version of B71 that have been designed with a higher mass and larger casing to increase the output at low frequencies (Radioear, 2015b). The lower resonance frequency, f_r, can be approximated to a function of the mass m and the spring stiffness k as

$$f_r \approx \frac{1}{2\pi}\sqrt{\frac{k}{m}}. \tag{3.2}$$

3.1.3 Radioear B81

To overcome the issues with distortion at low frequencies, a new type of bone vibrator has recently been developed under the trade name Radioear B81 (Radioear Corporation, Pennsylvania, USA) and is shown in Figure 3.3. Its motor unit is based on the balanced electromagnetic separation transducer (BEST) principle, which was first discovered by Håkansson (2003) in an attempt to improve the performance of conventional transducers and to make them smaller and more suitable to be used in hearing implants. The BEST principle was also found beneficial for BC audiometry as it was discovered to have an improved performance at low frequencies, where improvements are called for. A comprehensive description of the BEST principle is given in Håkansson (2003) and is summarized below.

3.1.4 The balanced electromagnetic separation transducer

The BEST principle is also a variable reluctance transducer type, but it uses four permanent magnets positioned in a way that the non-linear forces are

Figure 3.3: External view of the Radioear B81.

opposed and cancelled. This is achieved by a balance between two inner and two outer air-gaps. In each air-gap, a permanent magnet contributes with a static flux, Φ_0, and in the inner air-gaps, an additional time-varying flux, $\Phi_\sim$, is induced as a current flows through a coil that is winded around a bobbin core. The inner air-gaps are one upper and one lower, where Φ_0 are opposed by different directions of the permanent magnets, but $\Phi_\sim$ flows in the same direction. An illustration of the magnetic circuit of the BEST principle is shown in Figure 3.4, where A and D are the outer air-gaps and, B and C are the inner air-gaps. The time-varying and static flux pathways are outlined by dashed and solid lines, respectively, and it can be seen how half of the time-varying flux flows through each side. As the force in each air-gap is proportional to the total flux in the air-gap squared, the total flux to force relation of the transducer can be found by calculating the force proportionality in each air-gap and adding them together. Moreover, the force in air-gap A and D are

$$F_A = -F_D \propto \Phi_0^2, \tag{3.3}$$

and in air-gap B

$$F_B \propto (\Phi_0 - \frac{\Phi_\sim}{2})^2, \tag{3.4}$$

and in air-gap C

$$F_C \propto -(\Phi_0 + \frac{\Phi_\sim}{2})^2. \tag{3.5}$$

Using the symmetry for both sides, the total vibrating force of the transducer can be found by multiplying the force on one side by a factor of 2 as follows

$$F_{tot} = 2(F_A + F_B + F_C + F_D). \tag{3.6}$$

Finally, by inserting equations 3.3 to 3.5 in equation 3.6, the total vibrating force is proportional to

$$F_{tot} \propto 2(\Phi_0^2 + (\Phi_0 - \frac{\Phi_\sim}{2})^2 - (\Phi_0 + \frac{\Phi_\sim}{2})^2 - \Phi_0^2) = 4\Phi_0\Phi_\sim. \tag{3.7}$$

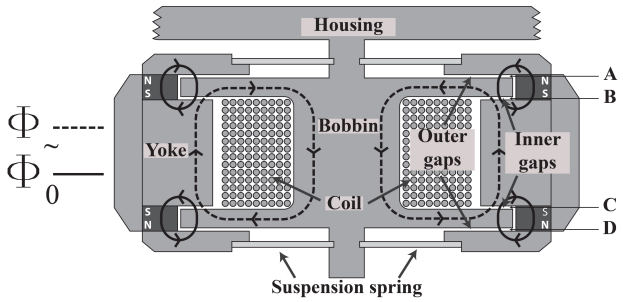

Figure 3.4: Cross-sectional view of the BEST design showing its permanent magnets and air gaps.

It is obvious from equation 3.7 that the flux to force relation is linear as both the static term Φ_0^2 and the second order distortion term $\Phi_\sim^2$ have been cancelled.

3.2 Bone conduction devices

3.2.1 Conventional devices

The only BCD type that does not require any surgery is the conventional BCD, which is its main advantage. It vibrates the skull bone via a transducer that is pressed against the skin using either a steel spring or a soft head band to achieve a static force that is required for efficient transmission, see Figure 3.5. This is the same technique that is used by audiometric bone vibrators except that the transducer in BCDs is driven by a battery operated AP with microphones instead of a power line operated audiometer. Unfortunately, there is a risk for skin complications due to the static force if the device is worn on a daily basis. Another challenge is the risk of feedback at high gain settings, which might require that the AP unit must be positioned on the contralateral ear. Furthermore, the skin does not transmit high frequencies as efficiently as low frequencies (Håkansson et al., 1984), which limits the rehabilitation in patients with mixed hearing loss, where higher gain is needed.

3.2.2 The bone anchored hearing aid

In the late 1970′s, the percutaneous bone anchored hearing aid (BAHA) was developed to overcome some of the issues with skin-driven conventional BCDs. Its transducer and AP are housed in the same unit and attached to a skin-penetrating abutment that is anchored in the skull bone using a titanium fixture, see Figure 3.6. Similar to dental implants, the titanium

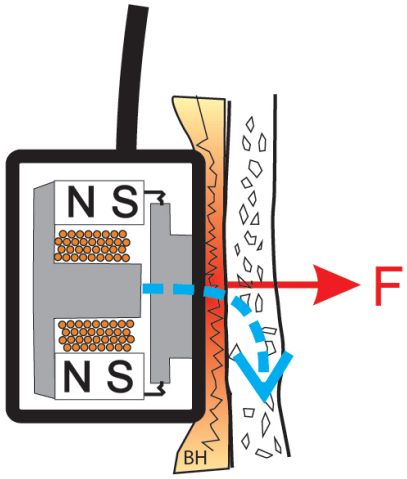

Figure 3.5: An illustration of the conventional bone conduction device that induces vibrations in the skull bone by a transducer that is, similar to bone vibrators, pressed against the skin with a static force F using a steel spring (Kompis and Caversaccio, 2011).

fixture is mounted into a drilled hole in the bone to achieve an osseointegrated attachment. The surgery is quick and safe and has been improved over the years by introducing new techniques to reduce skin complications (de Wolf et al., 2008; Hultcrantz and Lanis, 2014). In comparison with conventional BCDs, the BAHA offers a direct drive to the bone and thereby a more efficient transmission of high frequency sounds (Håkansson et al., 1984). As the high frequency performance is improved, both patients with conductive and mild-to-moderate mixed hearing loss can benefit from this device. However, some skin-complications can arise around the skin-penetrating abutment and this area requires daily care (Snik et al., 2005; Dun et al., 2012; Kiringoda and Lustig, 2013). Also, the challenge with feedback remains (Taghavi et al., 2012), even though it is more critical for conventional BCDs.

3.2.3 Transcutaneous devices

Today, the trend is moving towards transcutaneous BCDs that reduce the skin-related complications involved with conventional and percutaneous BCDs. Both passive and active solutions are commercially available on the market. The passive solutions are very similar to conventional BCDs, with the vibrations induced via the skin, but the static transducer pressure is established using permanent magnets instead of a steel spring or headband, see Figure 3.7. Even though the skin is intact, which is its main advantage, the high fre-

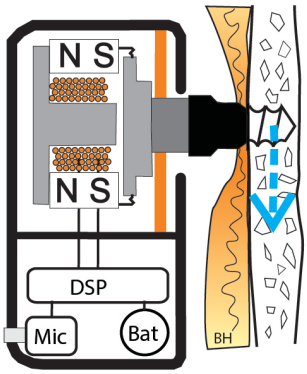

Figure 3.6: The percutaneous bone anchored hearing aid. It uses a battery driven transducer and audio processor unit coupled to a skin penetrating abutment screw that is fixed in the skull bone to achieve an osseointegrated and direct-bone-drive. A microphone picks up the sound and a digital sound processor controls the input to the transducer (Kompis and Caversaccio, 2011).

quency damping of the skin remains, feedback is not optimal and a relatively high retention force is required for efficient sound transmission.

The transducer in active transcutaneous BCDs is directly attached to the bone as in the BAHA, but the skin is kept intact in these devices and no permanent skin penetration is required. Instead, the sound is wirelessly transmitted as a modulated electromagnetic signal from a transmitter coil in the AP to a receiver coil in the implanted unit. The current in the receiver coil will then further drive the implanted transducer accordingly to the signal that was picked up by the microphones in the AP. To optimize the signal transmission of the link and for retention of the AP, the two coils are tuned and magnetically attached over each other using one permanent magnet in the center of each coil. In active transcutaneous BCDs, the microphone(s) are well separated from the transducer and with skin in-between, which makes it less prone to feedback.

3.2.4 The bone conduction implant

The bone conduction implant (BCI) is an active transcutaneous BCD developed in Göteborg, Sweden, by research groups at Chalmers University of Technology and Sahlgrenska University Hospital. It is currently under evaluation and verification in an ongoing clinical study approved by the Swedish Medical Agency and the Regional Ethical Review Board. The papers included in this thesis indicate that the BCI can provide sufficient rehabilitation for patients who are suffering from conductive or mild-to-moderate

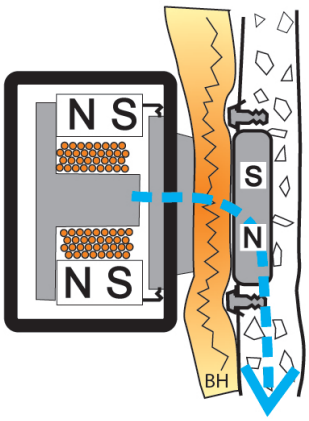

Figure 3.7: The principle design of a passive transcutaneous bone conduction device, where the vibrations are induced in the bone via the skin as similar to the conventional BCD except that it uses implanted magnets for retention instead of a steel spring or soft headband (Kompis and Caversaccio, 2011).

mixed hearing loss, and that it possibly tolerates magnetic resonance imaging at 1.5 Tesla.

The vital components BCI implant (transducer, electronics, and retention magnet) are sealed in hermetic titanium casings and the whole implant is sealed by an implant silicon grade, except the surface in contact with the skull bone for osseointegration. In Figure 3.8a, the principal design of the BCI system is shown and in Figure 3.8b the external view of the AP and the implanted unit. To drive the transducer, a current is induced in the receiver coil from a transmitter coil in the AP, which establishes the wireless induction link. The transducer is based on the BEST principle and is attached inside the titanium casing in a way that a high resonance frequency is created. The transducer casing is mounted in a 4-5 mm deep drilled recess of the mastoid part of the temporal bone in order to establish a flat surface attachment to the bone. Currently, the transducer casing is fixed by a titanium wire, but also other methods might be used, such as a titanium bar or sutures.

The AP comprises two microphones, a digital signal processor, modulation electronics, a retention magnet and a transmitter coil. Incoming sound to the microphones are transformed to an electrical signal, processed in an electrical filter and amplitude modulated to finally be transmitted in a carrier wave through the induction link to the implant. Before the received signal can drive the transducer, it is first demodulated from the carrier wave back to the original sound signal.

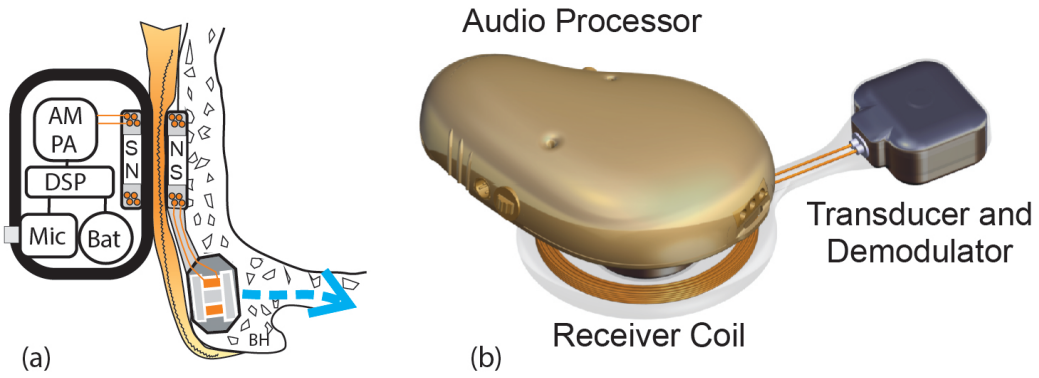

Figure 3.8: a) An illustration of the principal design and the components of the BCI system showing the audio processor with microphone, digital sound processor, power amplifier, amplitude modulatior, induction link and transducer (Kompis and Caversaccio, 2011). b) The external view of the BCI system.

Chapter 4

Summary of papers

4.1 Electro-acoustic performance of the new bone vibrator Radioear B81: A comparison with the conventional Radioear B71 (Paper I)

Diagnostic hearing investigations of patients with suspected hearing loss comprise both air and bone conduction threshold testing. The bone conduction threshold testing is used for assessing the degree of sensorineural hearing loss and has been performed using the Radioear B71 bone vibrator ever since the 1970′s. However, the B71 is known for its poor performance at low frequencies due to its conventional design with unbalanced air gaps that produces high distortion. In an attempt to improve the low frequency performance, the BEST principle was developed by Håkansson (2003). The BEST principle comprises two opposed, but balanced, air gaps so that non-linear distortion is reduced and higher output levels can be achieved. In a collaboration between Ortofon A/S, Nakskov, Denmark, and Chalmers University of Technology, Göteborg, Sweden, the BEST design has been further optimized and is now used in the motor unit of the new bone vibrator Radioear B81 and the motor unit as well as the casing and electrical contacts has been adapted for serial production.

The objective of the study presented in Paper I was to evaluate the electro-acoustic performance of the B81 in comparison with the B71. Frequency response, total harmonic distortion (THD), maximum output and electrical impedance were measured for six devices of each bone vibrator type on an artificial mastoid Brüel & Kjær 4930 where the bone vibrators

were attached with a static force of 5.4 N according to ISO 389-3 (1994). Compensation for the transmission through the pad on top of the gauge of the artificial mastoid was made by post processing in all measurements, see Appendix A for calibration details.

The frequency response of the B81 was designed to replicate the B71 and it was found that they were practically identical except for a small deviation at the mid frequencies where the B81 is 5.5 dB more efficient. Most importantly, it was found that the THD was considerably lower for the B81 up to 1000 Hz and mainly unchanged above when driven by a constant voltage of 1 V_{RMS}. The maximum hearing levels for the B81 were found to be 10.7 to 22.0 dB higher than for the B71 at frequencies below 1500 Hz and unchanged above. It was found that the B81 met the IEC 60645-1 requirements at all frequencies, but the B71 produced an output that was below the standard at 250 Hz. When the THD for the B71 is compensated for the actual hearing sensitivity of the harmonics, it is obvious that distortion at low frequencies is a serious problem where improvements are called for.

In conclusion, the new B81 may offer a new era in low frequency bone conduction audiometry as it allows higher hearing levels with less distortion than the B71 below 1500 Hz. In particular, bone conduction threshold testing at 250 Hz can now be used for routine diagnostics.

4.2 MRI Induced Torque and Demagnetization in Retention Magnets for a Bone Conduction Implant (Paper II)

Magnetic resonance imaging (MRI) is used as a diagnostic tool that uses magnetic fields for imaging of organs and internal structures of the human body. However, there are risks involved with MRI scanning of patients with implants, mainly related to the interaction with magnetic and electric conductive materials. The major safety concern for implants with implanted permanent magnets is discomfort or pain from implant movement, or in the worst case, dislocation. Paper II comprises an investigation of the torque and demagnetization effects on the retention magnet used in the bone conduction implant (BCI) when scanned in MRI. The aim of the study was to investigate these effects, both by experimental measurements in an electromagnet and by computer simulations using the software COMSOL Multiphysics 4.2 (COMSOL AB, Stockholm, Sweden).

The electromagnet generated a uniform magnetic field of 1.5 Tesla, similar to the field in a 1.5 Tesla MRI scanner. The stray-field around the electromagnet was considerably lower than in a MRI scanner because a dipole magnet with a closed magnetic circuit was used. This setup made the measurements easier as the electronic equipment can be used closer to the uniform field. The retention magnets in the BCI is a pair of two permanent magnets, one positioned internally in the implanted part, and one positioned in the externally worn audio processor (AP). When evaluating the safety aspects of the BCI during MRI, only the internal permanent magnet needs to be considered, since the patient can easily remove the AP before entering the MRI environment. In order to investigate how the choice of coercivity affects demagnetization and torque, two types of permanent magnets with the same size and magnetization, but different coercive field strengths were tested. One magnet had higher coercivity than 1.5 Tesla (standard BCI magnet) and one had lower coercivity. Demagnetization was calculated as the percentage loss in retention force against a reference magnet before and after exposure to the magnetic field.

The permanent magnet was positioned in the uniform field between the south and north pole of the electromagnet and fixed inside a cylindrical aluminum rod in order to be able to rotate the magnet inside the field. An angle potentiometer was attached at one end of the rod to measure the deflection angle. A force gauge measured the holding force required to keep it at different deflection angles and the torque was found by multiplying the holding force by the radius of a disc attached to the rod. The torque measurement was also simulated in COMSOL Multiphysics by defining a domain with a uniform field with appropriate size where a modelled permanent magnet was rotated and the electromagnetic torque was numerically calculated for each angle, see Appendix C for simulation details.

In the experiments, demagnetization and maximum torque for the high coercive field magnets were in average found to be 7.7 $\pm$ 2.5 % and 0.20 $\pm$ 0.01 Nm, respectively and 71.4 $\pm$ 19.1 % and 0.18 $\pm$ 0.01 Nm for the low coercive field magnets, respectively. The simulated maximum torque was 0.34 Nm which deviated from the measured torque in terms of amplitude. This deviation was assumed to relate to an insufficient magnet model that did not include demagnetization characteristics.

In conclusion it was found that the present design of the retention magnet in the BCI implant might meet the criteria to be MR conditional up to 1.5 Tesla in terms of magnetically induced torque and with only minor effects on demagnetization.

4.3 MRI Investigation of the Bone Conduction Implant - a pilot study at 1.5 Tesla (Paper III)

In patients who are using active medical devices, such as pacemakers, cochlear implants and other hearing implants, severe events can happen during MRI scanning, including patient injury and device break down. On top of that, a heavily distorted image can occur in the vicinity of the implant. In Paper III, the aim was to investigate if the present design of the full BCI withstands MRI at 1.5 Tesla. In particular, to compare maximum power output (MPO), THD and retention force before and after MRI as well as to evaluate the image artifact when the implant is attached over the skin on a test persons head.

In this study, the transducer of the BCI is pressed against the skin on a test person similar to the pressure of a conventional bone conduction device, so that vibrations from the transducer are induced through the skin into the skull bone. This procedure made it possible for the test person to listen via the implant to first see if an annoying sound is induced by the magnetic fields during MRI and also to verify its function when driven by the AP afterwards. One BCI implant was thus placed over the skin on a test person at the assumed location for implantation and then scanned in a 1.5 Tesla MRI scanner. Images were attained both with and without the implant, in three orthogonal planes and for spin-echo (SE) and gradient-echo (GE) pulse sequences.

It was found that the exposure of 1.5 Tesla had only a minor effect on the MPO (decreased with an average of 1.1 $\pm$ 2.1 dB) and the THD remained unchanged above 300 Hz. The retention magnet was subjected to a minor demagnetization (5% loss of force) and the test person did not hear any MRI induced sound nor felt any movement of the implant. The maximum size of the image artifact was measured as the maximum distance from the implant in the sagittal, coronal and axial plane and found to be 9, 10 and 9 cm for the GE pulse sequence and 8, 9 and 8 cm for the SE pulse sequence, respectively. It is clear from this study that image artifacts distort the image in the vicinity of the implant, eliminating the possibility to visualize tissue properties in this region.

In the implanted unit of the BCI, the retention magnet is connected with a relatively stiff titanium bar to the transducer casing that is rigidly attached to the bone. This is assumed to prevent the magnet from moving and a head bandage around the head might not be needed, even if it may be recom-

mended for extra caution.

In summary, it was found in this study that the current BCI design may pass an approval to be MR conditional up to 1.5 Tesla.

4.4 Technical Design of a New Bone Conduction Implant (BCI) System (Paper IV)

The emphasis in Paper IV is to present the basic technical design of the BCI system; in general, how it has been developed to improve audiological and life quality outcomes for its patients, seen from a technical perspective; and in particular, how the induction link was optimized to transmit sound with robust efficiency for most patients. The technical performance of the BCI system has been verified by measurements on dry skull, on skull simulator, in animal model (sheep), on cadaver heads, and finally implanted in humans. In this paper, the BCI design used in an on-going clinical study on the first six patients is described and technically verified by measurements of retention force, MPO, THD and current consumption.

As the skin thickness varies among patients, it requires that the output is desensitized for different distances between the receiver and transmitter coils in the induction link to offer the same performance for all patients. Also, the retention magnet system needs to be designed to meet the skin thickness variations. The target retention force lies between 0.4 and 1 N and if a weaker or stronger force is needed, a series of different magnet strengths are available to compensate for this in the external unit. Furthermore, to fit the AP to the hearing loss of a particular patient, a versatile digital sound processor with different programs to choose from is used.

The maximum output force was found to be 107 dB re. 1 μN at a skin thickness of 5 mm and with a maximum change of 1.5 dB for skin thicknesses between 2 to 8 mm. To achieve high output force levels for both the lower and upper frequencies, the transducer is designed with two damped resonance peaks in the range of 750 to 800 and 4500 to 5000 Hz, respectively. By using an ultra-low power ASIC, the current consumption is decreased to 7.5 mA, which makes the battery last for about 5-7 days depending on usage. Furthermore, the THD was found to be below 8% in the speech frequency range at an input level of 70 dB SPL.

In summary, it was found that the BCI offers sufficiently output force levels and excellent signal quality.

4.5 The Bone Conduction Implant - Clinical results of the first six patients (Paper V)

The BCI is an active transcutaneous BCD with the transducer surgically implanted in the mastoid part of the temporal bone under intact skin. Paper V summarizes the clinical results of the first six BCI patients after 6 months in an on-going clinical study, approved by the Swedish Medical Agency and the Regional Ethical Review Board. From experience of these first patients, the surgical procedure is confirmed to be straight forward, safe and uncomplicated. The aim of this study was to investigate the patients' audiological and quality of life outcomes by comparing with the unaided condition and with a BAHA on a softband. The BCI offers a direct and osseointegrated bone drive, while the BAHA on softband is placed externally on the head with skin in-between the transducer and bone. To compensate the BAHA (Ponto Pro Power, Oticon Medical, Askim, Sweden) for the transmission thru the skin, up to 10 dB extra gain was added to the higher frequencies for the BAHA on softband by using a software for the fitting procedure based on in-situ BC thresholds. In addition, automatic functions like adaptive noise reduction, directional microphones and feedback reduction were all disabled on both devices to prevent them from affecting the results.

The patients' audibility were tested using warble tones, speech recognition in quiet and in noise and from intelligibility tests. The quality of life outcomes were conducted in addition to the audiometric testing as a subjective measure by using Swedish APHAB and GBI questionnaires. The APHAB covers four categories: ease of communication, listening against background noise, listening under reverberant conditions and aversiveness of sound. The GBI evaluates the patient benefit in general, social support and physical health where the results are scores on a scale from -100 to +100 and positive scores indicate a benefit in quality of life.

A statistically significant improvement (α=0.05) with the BCI over the unaided condition was found in all audiometric tests and questionnaires. The average improvement in hearing thresholds was found to be 31.0 dB, speech recognition threshold 27.0 dB and speech recognition score in noise 51.2%. The signal to noise ratio at speech level for the BCI was found to be -5.5 dB. Audiometric results as well as the subjective measures of quality of life were similar or better with the BCI as compared with BAHA on softband.

In summary, the results from the first six patients indicate that patients with conductive or mild-to-moderate mixed hearing loss will have a significant hearing rehabilitation with the BCI.

Chapter 5

Conclusions and future work

Over the years, the variety of devices has increased in the field of bone conduction hearing and today there is a wide range of possibilities offered when it comes to both audiometry and rehabilitation of hearing loss. In the transition from conventional devices, the trend is towards audiometric devices with improved low frequency performance and hearing implants with transcutaneous solutions that keep the skin intact. In this thesis, the main conclusions are:

- **The Radioear B81 (Paper I)** was found to generate less harmonic distortion and allow higher output levels than the B71 below 1500 Hz by using the BEST principle. It was also verified to be compatible with the same audiometers as the B71 with almost identical frequency response and electrical impedance. The B81 allows for routine bone conduction diagnostics to be performed at 250 Hz, which has rarely been done with the B71 before.

- **The BCI retention magnet (Paper II)** was only demagnetized by 7.7% and experienced a maximum torque of 0.20 Nm, when exposed to a uniform magnetic field of 1.5 Tesla. Based on these results, the BCI implant is anticipated to pass the requirements for approval as MR conditional up to 1.5 Tesla if a compression band is used around the skull to avoid movement of implant.

- **The BCI system in 1.5 Tesla MRI (Paper III)** was investigated in a pilot study using one implant positioned externally over the skin on a test person′s head in order to replicate the real case scenario where it is positioned under the skin. The study indicated that no induced BC sound was heard, and the effects on output force, distortion and

retention force were minor, but the image was distorted in the vicinity of the implant to a maximum distance of 10 cm. Most importantly, it was found that the current BCI design may pass an approval to be MR conditional up to 1.5 Tesla.

- **The BCI system technical design (Paper IV)** was technically verified to generate sufficiently high output force levels with low THD and to offer the same output power for patients regardless of different skin flap thickness. With its ultra-low power ASIC design, the current consumption is kept low and the battery lasts for about 5-7 days depending on the patient use. The overall conclusion is that the BCI design can be a realistic alternative to BAHA.

- **The BCI clinical study (Paper V)** of the first six patients showed a significant improvement with the BCI over the unaided condition and, in comparison with BAHA on softband (skin drive), the BCI provides either similar or better rehabilitation for patients with conductive or mild-to-moderate mixed hearing loss. Also, the surgery is straightforward, safe and uncomplicated.

In future studies of the Radioear B81, other aspects including acoustically radiated noise from the bone vibrator casing, static force dependence, drop testing, and tactile thresholds are of interest to investigate. Today, it is unknown if B81 will replace B71 completely or remain as an alternative with better performance for BC audiometry at low frequencies.

The current technical design of the BCI system is used in the implants of the first six patients in an ongoing clinical study. The aim of the clinical study is to gather evidence for CE-approval as a next step for becoming commercially available. This might require design changes in order to comply with different standard requirements and for an efficient serial production. One such requirement is for the implant to withstand mechanical stress from rough handling after manufacturing, during packaging, transportation and surgery, and to determine the expected lifetime for the implant. These aspects in future studies. The results in the clinical study (Paper V) are based on measurements performed at 6-month follow-up visits, meaning that longer follow-up time as well as data from more patients will contribute to more definite results in the future.

Regarding the safety of performing MRI of patients that are using the BCI implant, which was studied in Paper II and III, more implants and test subjects, as well as different pulse sequences and manufacturers, should be tested in the future. Furthermore, if patients regularly need to perform MRI, the effects of repetitive exposure have to be considered. For comparison reasons

of the torque experiments in Paper II, the study also included a simulation part where it was found that the maximum induced torque (0.34 Nm) was higher than in the experiments (0.20 Nm). This overestimation is assumed to relate to an insufficient model of the retention magnet in the simulation program that does not include demagnetization characteristics. In the future, a more extensive simulation model of the retention magnet is therefore recommended, also for studies at fields higher than 1.5 Tesla where experimental measurements are more difficult to perform. The focus in future MRI related studies will be to further investigate the requirements for passing approval at 1.5 and 3 Tesla MRI, both by simulation and experiments.

Appendices

Appendix A

Calibration

When the electro-acoustic performance of a bone vibrator is evaluated, measurement instruments with specific filter characteristics require calibration. Therefore, the measurement setup used in Paper I, both the artificial mastoid and the charge amplifier need to be calibrated.

The output signal from the artificial mastoid is a voltage V_{out} that is generated when a force F_{in} is applied on the surface of the rubber pad, see Figure A.1. When F_{in} is a sinus signal with the amplitude 1 N and the frequency 1000 Hz, V_{out} should have an amplitude of 120 mV according to the calibration sheet of the artificial mastoid. This force to voltage relation is commonly referred to as the force sensitivity constant α and is equal to 120 mV/N. It specifies the sensitivity at 1 kHz and is sometimes used to determine the sensitivity for the total frequency range of the artificial mastoid between 100 and 10 000 Hz, which must be taken into account. This frequency dependence is commonly referred to as the pad correction curve $P(j\omega)$ (FigureA.2) and is defined as the ratio between $F_{in}(j\omega)$ and $V_{out}(j\omega)$ as follows

$$P(j\omega) = \frac{F_{in}(j\omega)}{V_{out}(j\omega)}. \tag{A.1}$$

The pad correction is then used to determine the frequency spectrum of $F_{in}(j\omega)$ of the bone vibrator, from which the total harmonic distortion (THD) and the frequency response $G(j\omega)$ can be calculated. The frequency response of the bone vibrator is given by the input voltage $V_{in}(j\omega)$ to $F_{in}(j\omega)$,

$$G(j\omega) = \frac{F_{in}(j\omega)}{V_{in}(j\omega)} = \frac{P(j\omega)V_{out}(j\omega)}{V_{in}(j\omega)}. \tag{A.2}$$

The pad correction curve can be measured using an impedance head between a minishaker and the artificial mastoid. There are two output signals from

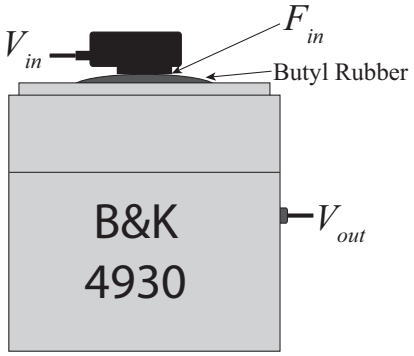

Figure A.1: Attachment of the bone vibrator on the artificial mastoid. The input voltage to the bone vibrator is V_{in}, which applies a force F_{in} to the rubber pad so and generates an output voltage V_{out} from the artificial mastoid.

the impedance head, $A(j\omega)$ and $F(j\omega)$. First, the shape $P'(j\omega)$ of the pad correction curve has to be found and then it is scaled to intersect α=120 mV/N at 1000 Hz so that $P(j2\pi1000) = \alpha$ and

$$P(j\omega) = \alpha \frac{P'(j\omega)}{P'(j2\pi1000)}, \tag{A.3}$$

where

$$P'(j\omega) = \frac{F'_{in}(j\omega)}{V_{out}(j\omega)}. \tag{A.4}$$

The primed input force $F'_{in}(j\omega)$ has the shape of $F_{in}(j\omega)$ and should be scaled with a sensitivity constant to give the correct force. This constant is unknown because the sensitivity constants for the output signals from the impedance head are often uncalibrated. However, the ratio between $F(j\omega)$ and $A(j\omega)$, denoted K, can easily be found and is enough information for finding $P(j\omega)$ if at least α is known. In the time domain, velocity is the integrated acceleration, which corresponds to $A(j\omega)/j\omega$ in the frequency domain, and this ratio should be multiplied by the mechanical impedance $Z_m(j\omega)$ of the artificial mastoid to give the force

$$F_{in}(j\omega) = \frac{A(j\omega)}{j\omega} Z_m(j\omega). \tag{A.5}$$

The acceleration signal from the impedance head is the unscaled acceleration, denoted $A'(j\omega)$, and is measured as a voltage rather than an acceleration. This gives the measured and unscaled input force

$$F'_{in}(j\omega) = \frac{A'(j\omega)}{j\omega} Z_m(j\omega). \tag{A.6}$$

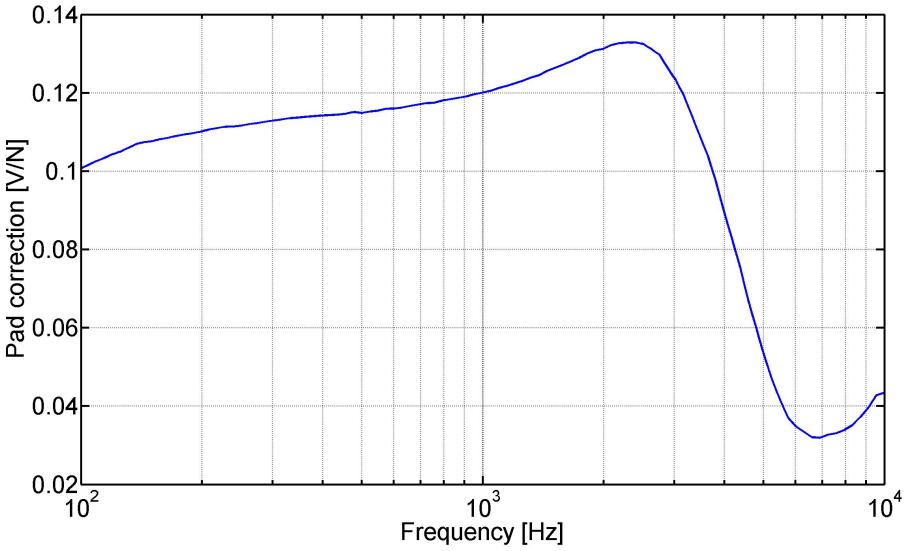

Figure A.2: The pad correction curve of the artificial mastoid BK 4930

Inserting equation (A.6) in (A.4) then gives

$$P(j\omega)' = \frac{A'(j\omega)}{j\omega}\frac{Z_m(j\omega)}{V_{out}(j\omega)}. \tag{A.7}$$

Inside the impedance head there is an inherently mass m_0=1.1 g below a force gauge, which has a mechanical impedance $Z_0(j\omega)$=$j\omega m_0$ that is mechanically coupled in series with $Z_m(j\omega)$. Therefore, $F(j\omega)$ acts on m_0 in series with the artificial mastoid, while $F_{in}(j\omega)$ is only the force on the rubber pad, which gives that

$$F(j\omega) = \frac{A(j\omega)}{j\omega}\left(Z_0(j\omega) + Z_m(j\omega)\right) = \frac{A(j\omega)}{j\omega}\left(j\omega m_0 + Z_m(j\omega)\right), \tag{A.8}$$

and the mechanical impedance of the artificial mastoid becomes

$$Z_m(j\omega) = j\omega\left(\frac{F(j\omega)}{A(j\omega)} - m_0\right), \tag{A.9}$$

see Figure A.3. The input force $F_{in}(j\omega)$ to the rubber pad should not be confused with the output force $F(j\omega)$ from the impedance head. Furthermore, the sensitivity constant for $F(j\omega)$ is uncalibrated and the voltage measured from the force gauge of the impedance head is an unscaled force, denoted $F'(j\omega)$. By using the ratio K, neither the acceleration nor the force sensitivity constants are needed, which gives

$$Z_m(j\omega) = j\omega\left(\frac{F'(j\omega)}{A'(j\omega)}K - m_0\right), \tag{A.10}$$

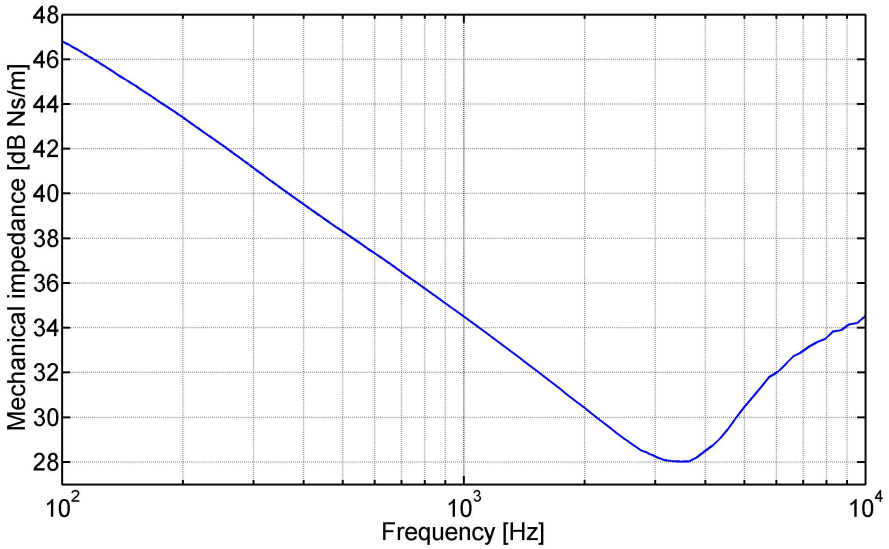

Figure A.3: The mechanical impedance of the artificial mastoid BK 4930

where K is a property of the impedance head that has to be determined in a separate measurement by connecting the impedance head to the minishaker and load it with a known mass m. This mass will be mechanically coupled in series with m_0 and the output force $F(j\omega)$ will act on those two masses so that

$$F(j\omega) = \frac{A(j\omega)}{j\omega}\left(j\omega m_0 + j\omega m\right), \tag{A.11}$$

which implies that the ratio between $F(j\omega)$ and $A(j\omega)$ will be the total mass so that

$$\frac{F(j\omega)}{A(j\omega)} = m_0 + m. \tag{A.12}$$

If the frequency response from the measured voltages $A'(j\omega)$ to $F'(j\omega)$ is not equal to the total mass, it should be corrected by K so that

$$\frac{F'(j\omega)}{A'(j\omega)}K = m_0 + m. \tag{A.13}$$

Then K can be calculated as

$$K = \frac{A'(j\omega)}{F'(j\omega)}\left(m_0 + m\right). \tag{A.14}$$

When K is to be determined, a relatively small mass should be used so that a flat frequency response is achieved at the lower frequencies and not influenced by the resonance peak.

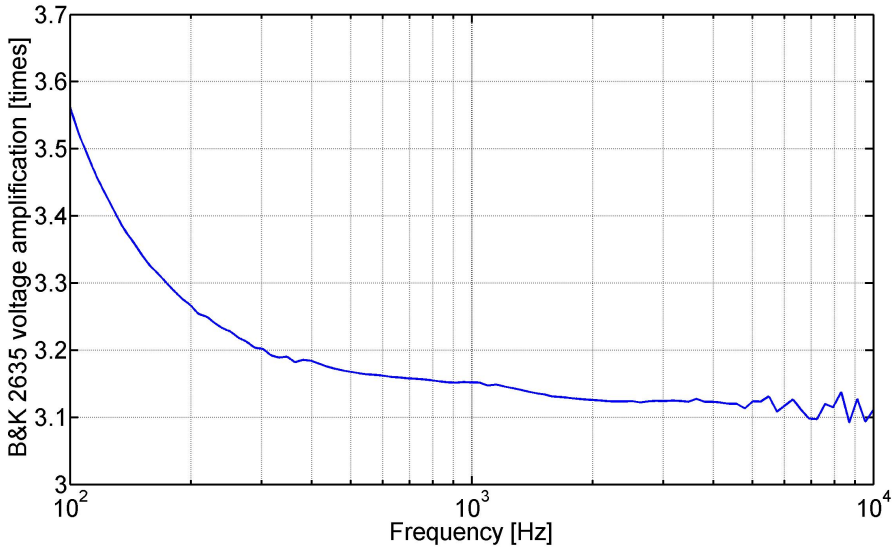

Figure A.4: The voltage amplification of the charge amplifier BK 2635

To compensate for the filter characteristics $H(j\omega)$ of the charge amplifier (Figure A.4), the difference in frequency response of a bone vibrator measured with $(Y(j\omega))$ and without $(X(j\omega))$ the amplifier, were found to be

$$H(j\omega) = \frac{Y(j\omega)}{X(j\omega)}. \tag{A.15}$$

A summary of the calibration process of the artificial mastoid is given below:

- First, obtain K by adding a mass on top of the impedance head when it is attached to the minishaker and measure

$$K = \frac{A'(j\omega)}{F'(j\omega)} (m_0 + m) .$$

- Remove the added mass and attach the minishaker and impedance head upside down on the rubber pad of the artificial mastoid with 5.4 N. Obtain $Z_m(j\omega)$ by measuring

$$Z_m(j\omega) = j\omega \left(\frac{F'(j\omega)}{A'(j\omega)} K - m_0 \right) .$$

- Keep $Z_m(j\omega)$ (Figure A.3) and measure the unscaled pad correction curve $P'(j\omega)$ as

$$P(j\omega)' = \frac{A'(j\omega)}{j\omega} \frac{Z_m(j\omega)}{V_{out}(j\omega)}.$$

- Finally, scale the curve to intersect α=120 mV/N at 1 kHz.

$$P(j\omega) = \alpha \frac{P'(j\omega)}{P'(j2\pi 1000)}.$$

- The dynamic force acting on the rubber pad can now be found by measuring the output voltage $V_{out}(j\omega)$ and multiplying it with the pad correction curve, which gives

$$F_{in}(j\omega) = P(j\omega) V_{out}(j\omega).$$

- The frequency response $G(j\omega)$ of the bone vibrator that relates the input voltage $V_{in}(j\omega)$ to the input force $F_{in}(j\omega)$ can be found as

$$G(j\omega) = \frac{F_{in}(j\omega)}{V_{in}(j\omega)} = \frac{P(j\omega) V_{out}(j\omega)}{V_{in}(j\omega)}.$$

Appendix B

Disc magnet **B**-field equation

This appendix summarizes how the derivation of a uniformly magnetized circular cylinder given in Cheng (1989), was applied to the retention magnet of the BCI implant to determine equation (1) in the part of Paper II where the magnetically induced torque at 1.5 Tesla was simulated.

An object with a magnetic dipole moment has a magnetization vector $\mathbf{M}$. The partial scalar magnetic potential from each volume element at radial distance R is

$$dV_m = \frac{\mathbf{M}\cdot\hat{\boldsymbol{R}}}{4\pi R^2}, \tag{B.1}$$

where $\hat{\boldsymbol{R}}$ is the radial unit vector. Integration over the magnetized object's volume V' gives the total magnetic potential V_m as

$$V_m = \frac{1}{4\pi}\int_{V'} \frac{\mathbf{M}\cdot\hat{\boldsymbol{R}}}{R^2} dv'. \tag{B.2}$$

In cartesian coordinates, the radial distance R from the primed source point (x', y', z') to the fixed field point (x, y, z) can be written as

$$R = \sqrt{(x-x')^2 + (y-y')^2 + (z-z')^2}, \tag{B.3}$$

and the gradient of $1/R$ with respect to the primed coordinates is

$$\nabla'\left(\frac{1}{R}\right) = \frac{\hat{\boldsymbol{R}}}{R^2}. \tag{B.4}$$

Then the following vector identity can be used

$$\nabla'\cdot\left(\frac{1}{R}\right)\mathbf{M} = \left(\frac{1}{R}\right)\nabla'\cdot\mathbf{M} + \mathbf{M}\cdot\nabla'\left(\frac{1}{R}\right). \tag{B.5}$$

Inserting equation (B.5) in (B.2) gives the following expression for the magnetic potential

$$V_m = \frac{1}{4\pi}\left[\int_{V'} \nabla' \cdot \left(\frac{\mathbf{M}}{R}\right) dv' - \int_{V'} \frac{\nabla' \cdot \mathbf{M}}{R} dv'\right]. \tag{B.6}$$

By applying the divergence theorem on the first integral in equation B.6, it can be written as a surface integral over the magnetized object's surface S' and the new expression becomes

$$V_m = \frac{1}{4\pi}\oint_{S'} \frac{\mathbf{M}\cdot\hat{\boldsymbol{n}}'}{R} ds' + \frac{1}{4\pi}\int_{V'} \frac{-\left(\nabla' \cdot \mathbf{M}\right)}{R} dv', \tag{B.7}$$

where $\hat{\boldsymbol{n}}'$ is the normal vector to the surface of the magnetized object. Introducing equivalent charge densities $\rho_{ms} = \mathbf{M}\cdot\hat{\boldsymbol{n}}'$ and $\rho_m = -\nabla' \cdot \mathbf{M}$ gives

$$V_m = \oint_{S'} \frac{\rho_{ms}}{4\pi R} ds' + \int_{V'} \frac{\rho_m}{4\pi R} dv'. \tag{B.8}$$

For a cylindrical disc shaped magnet with the axial magnetization $\mathbf{M}=\hat{\boldsymbol{z}}M_0$ the charge densities becomes

$$\rho_{ms} = \begin{cases} M_0 & \text{on the top surface,} \\ -M_0 & \text{on the bottom surface,} \\ 0 & \text{on the side wall;} \end{cases}$$

$$\rho_m = 0 \qquad \text{in the interior.}$$

With surface charge densities located at the top and bottom of the magnet, the magnetic potential from the positive surface charges at distance R_+ is

$$V_{m+} = \frac{M_0 \pi b^2}{4\pi R_+}, \tag{B.9}$$

and for the negative surface charges at distance R_-

$$V_{m-} = -\frac{M_0 \pi b^2}{4\pi R_-}. \tag{B.10}$$

Then the total magnetic potential becomes

$$V_T = \frac{q_m}{4\pi}\left(\frac{1}{R_+} - \frac{1}{R_-}\right), \tag{B.11}$$

where $q_m = M_0 \pi b^2$. To simplify the expression in equation (B.11) and under the assumption that $R \gg b$, the distances R_+ and R_- can be approximated as

$$\frac{1}{R_+} \cong \left(R - \frac{L}{2} \cos\theta \right)^{-1} \cong R^{-1} \left(1 + \frac{L}{2R} \cos\theta \right) \tag{B.12}$$

and

$$\frac{1}{R_-} \cong \left(R + \frac{L}{2} \cos\theta \right)^{-1} \cong R^{-1} \left(1 - \frac{L}{2R} \cos\theta \right). \tag{B.13}$$

By inserting equations (B.12) and (B.13) in (B.11), the final expression for V_T will be

$$V_T \cong \frac{q_m L \cos\theta}{4\pi R^2} = \frac{(\pi b^2 M_0)\, L \cos\theta}{4\pi R^2} = \frac{M_T \cos\theta}{4\pi R^2}, \tag{B.14}$$

where $M_T = q_m L = M_0 \pi b^2 L$ is the total dipole moment of the cylindrical magnet and the vectorized $\mathbf{B}$ field will thus be determined by

$$\mathbf{B} \cong -\mu_0 \nabla V_T = \frac{\mu_0 M_T}{4\pi R^3} \left(\hat{\boldsymbol{R}} 2\cos\theta + \hat{\boldsymbol{\theta}} \sin\theta \right), \tag{B.15}$$

which is equal to equation (1) in the simulation part of Paper II.

Appendix C

Simulations

The static magnetically induced torque on the retention magnet of the BCI implant was simulated in Paper II using COMSOL Multiphysics 4.2 (COMSOL AB, Stockholm, Sweden) which is a software that can approximate solutions to electromagnetic problems using the finite element method. The retention magnet was modelled as a cylindrical disc with a remanent flux density of 1.08 Tesla in the axial direction and with a relative permeability of 1.05, both specified by the manufacturer. The inside of the MRI scanner was modelled as a sphere of air in a uniform background field of 1.5 Tesla. In experiments like these, the magnetic field representing the inside of the MRI scanner has in practice a fixed direction and the measureing object is rotated to measure the torque at different angles. In the simulation, the magnet was instead fixed and the direction of the background field rotated around the magnet in a parametric sweep from 0 to 180^o with a step of 10^o. The simulation resulted in a sine function in the interval of $0 \leq \alpha \leq 180^o$ with the maximum value of 0.337 Nm at 90^o (Figure C.1) and with a discretization error less than 0.6%.

The simulation domain was defined with respect to the magnetic flux density at the distance R from the permanent magnet which must be zero at the periphery of the sphere in order to include the total field in the numerical calculation. The mathematical expression for the flux density around a cylindrical disc shaped permanent magnet (Appendix B) is given by

$$\mathbf{B} \cong \frac{\mu_0 M_T}{4\pi R^3} \left(\hat{\boldsymbol{R}} 2\cos\theta + \hat{\boldsymbol{\theta}} \sin\theta \right), \tag{C.1}$$

and comprises one radial and one angular component expressed by the unit vectors $\hat{\boldsymbol{R}}$ and $\hat{\boldsymbol{\theta}}$, repectively.

The magnetization M_T of the magnet is given in A/m and the angular position θ in radians. The zero boundary condition, which is fulfilled when

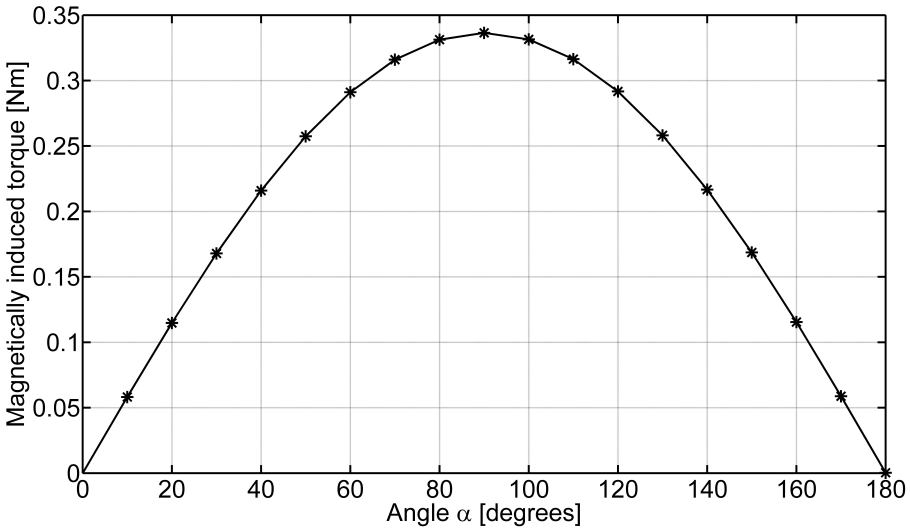

Figure C.1: Simulated static magnetic induced torque on the retention magnet of the BCI implant. A static uniform magnetic field of 1.5 Tesla was applied for angles between 0 and 180^o.

the radius of the sphere is large enough, implies that the radial component becomes zero when $R = R_{sphere}$ so that

$$\mathbf{B}(R_{sphere}) \cong \hat{\boldsymbol{R}} \frac{2\mu_0 M_T \cos\theta}{4\pi R_{sphere}^3} = 0. \tag{C.2}$$

In order to find the optimal value of Rsphere, it was swept from 5 cm to 15 cm with a step of 1 cm and the maximum torque was found to have a maximum variation less than 0.01% between 7 and 15 cm. This variation is small compared to the discretization error (0.6%) and there is no need to make R_{sphere} bigger than 7 cm.

The mesh resolution was required to be higher close to the magnet where the field lines changes more rapidly than at the boundary of the sphere where the mesh can be coarser. Furthermore, both the maximum and minimum element size was refined until the discretization error was less than 1%. In addition, an extrapolation to zero cell size was performed using values from numerical computations where the minimum cell size was decreased from 2.8 to 0.25 μm, which resulted in a torque of 0.3385 Nm, see Figure C.2. Finally, with a discretization error less than 1%, the significant simulated torque was 0.34 Nm which is the simulation result presented in Paper II.

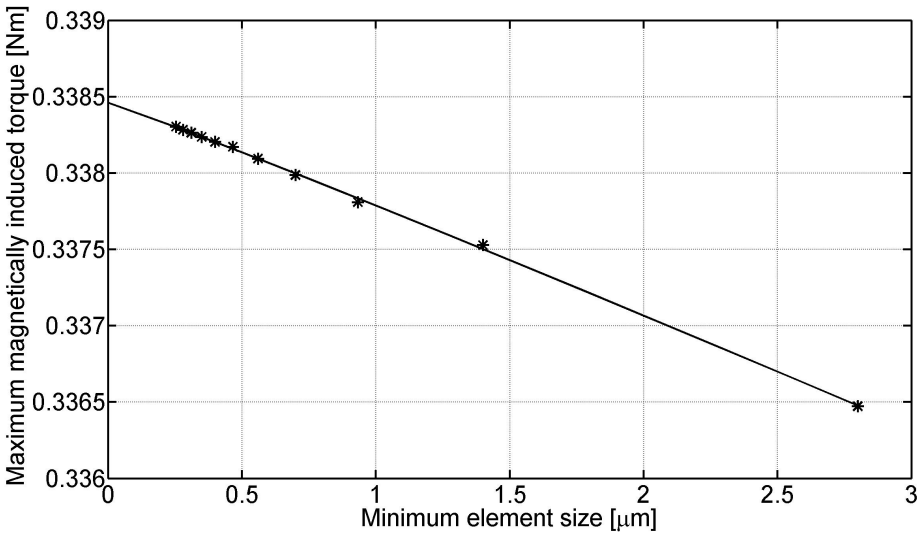

Figure C.2: The extrapolated curve (solid line) of the expected simulated magnetically induced torque when the cell size goes to zero. The simulated maximum magnetically induced torque ($*$) was swept for 10 exponentially distributed values of the minimum element size of the mesh.

Bibliography

Beltrame, A. M., Martini, A., Prosser, S., Giarbini, N., and Streitberger, C. (2009). Coupling the vibrant soundbridge to cochlea round window: auditory results in patients with mixed hearing loss. *Otology & Neurotology*, 30(2):194–201.

Bushong, S. C. (2003). *Magnetic resonance imaging: physical and biological principles, 3rd edition*. Elsevier Health Sciences.

Cheng, D. K. (1989). *Field and wave electromagnetics*, volume 2. Addison-wesley New York.

Clark, J. G. (1981). Uses and abuses of hearing loss classification. *Asha*, 23(7):493–500.

Coey, J. M. (2010). *Magnetism and magnetic materials*. Cambridge University Press.

de Wolf, M. J., Hol, M. K., Huygen, P. L., Mylanus, E. A., and Cremers, W. (2008). Nijmegen results with application of a bone-anchored hearing aid in children: simplified surgical technique. *Annals of Otology, Rhinology & Laryngology*, 117(11):805–814.

Dun, C. A., Faber, H. T., de Wolf, M. J., Mylanus, E. A., Cremers, C. W., and Hol, M. K. (2012). Assessment of more than 1,000 implanted percutaneous bone conduction devices: skin reactions and implant survival. *Otology & Neurotology*, 33(2):192–198.

Gallichan, M.-C., Ravenna, S., Giguere, C., Leroux, T., Wu, L., and Wong, G. S. (1998). High-frequency bone conduction audiometry using a piezoelectric transducer. *Canadian Acoustics*, 26(3):70–71.

Haacke, E. M., Brown, R. W., Thompson, M. R., and Venkatesan, R. (1999). *Magnetic resonance imaging: physical principles and sequence design*. John Wiley & Sons.

Håkansson, B., Tjellström, A., and Rosenhall, U. (1984). Hearing thresholds with direct bone conduction versus conventional bone conduction. *Scand. Audiol.*, 13:3–13.

Håkansson, B. E. (2003). The balanced electromagnetic separation transducer: A new bone conduction transducer. *The Journal of the Acoustical Society of America*, 113(2):818–825.

Hultcrantz, M. and Lanis, A. (2014). A five-year follow-up on the osseointegration of bone-anchored hearing device implantation without tissue reduction. *Otology & Neurotology*, 35(8):1480–1485.

ISO 389-3 (1994). *Acoustics - Reference zero for the calibration of audiometric equipment. Part 3: Reference equivalent threshold force levels for pure tones and bone vibrators.* Geneva: ISO; 1994-10-01.

Jesacher, M. O., Kiefer, J., Zierhofer, C., and Fauser, C. (2010). Torque measurements of the ossicular chain: implication on the mri safety of the hearing implant vibrant soundbridge. *Otology & Neurotology*, 31(4):676–680.

Kiringoda, R. and Lustig, L. R. (2013). A meta-analysis of the complications associated with osseointegrated hearing aids. *Otology & Neurotology*, 34(5):790–794.

Kompis, M. and Caversaccio, M.-D. (2011). *Implantable bone conduction hearing aids*, volume 71. Karger Medical and Scientific Publishers.

McComb, C., Allan, D., and Condon, B. (2009). Evaluation of the translational and rotational forces acting on a highly ferromagnetic orthopedic spinal implant in magnetic resonance imaging. *Journal of Magnetic Resonance Imaging*, 29(2):449–453.

MED-EL (2014). Vibrant soundbridge system. `http://s3.medel.com.s3.amazonaws.com/pdf/28477_10_Factsheet%20VSB%20System%20%28english%29-8seitig_screen6.pdf`. [Online; accessed 20-Dec-2014].

Nyenhuis, J. A., Park, S.-M., Kamondetdacha, R., Amjad, A., Shellock, F. G., and Rezai, A. R. (2005). Mri and implanted medical devices: basic interactions with an emphasis on heating. *Device and Materials Reliability, IEEE Transactions on*, 5(3):467–480.

Radioear (2015a). B71W Bone transducers. `http://radioear.us/pdfs/RE_B71W_LR.pdf`. [Online; accessed 16-Feb-2015].

Radioear (2015b). B72 Bone Transducers. `http://radioear.us/bone-transducers.html`. [Online; accessed 16-Feb-2015].

Reinfeldt, S., Håkansson, B., Taghavi, H., and Eeg-Olofsson, M. (2015). New developments in bone-conduction hearing implants: a review. *Medical devices (Auckl, NZ)*, 16(8):79–93.

Richards, W. D. and Frank, T. (1982). Frequency response and output variations of radioear b-71 and b-72 bone vibrators. *Ear and hearing*, 3(1):37–38.

Shellock, F. G. (2012). *Reference manual for magnetic resonance safety, implants and devices*. Biomedical research publishing group.

Shellock, F. G., Kanal, E., and Gilk, T. B. (2011). Regarding the value reported for the term âspatial gradient magnetic fieldâ and how this information is applied to labeling of medical implants and devices. *American Journal of Roentgenology*, 196(1):142–145.

Snik, A. F., Mylanus, E., Proops, D. W., Wolfaardt, J. F., Hodgetts, W. E., Somers, T., Niparko, J. K., Wazen, J. J., Sterkers, O., Cremers, C., et al. (2005). Consensus statements on the baha system: where do we stand at present? *The Annals of otology, rhinology & laryngology. Supplement*, 195:2–12.

Stenfelt, S. and Goode, R. L. (2005). Bone-conducted sound: Physiological and clinical aspects. *Otology Neurotology*, 26:1245–1261.

Taghavi, H., Håkansson, B., Reinfeldt, S., Eeg-Olofsson, M., and Akhshijan, S. (2012). Feedback analysis in percutaneous bone-conduction device and bone-conduction implant on a dry cranium. *Otology & Neurotology*, 33(3):413–420.

Teissl, C., Kremser, C., Hochmair, E. S., and Hochmair-Desoyer, I. J. (1998). Cochlear implants: in vitro investigation of electromagnetic interference at mr imaging–compatibility and safety aspects. *Radiology*, 208(3):700–708.

Todt, I., Wagner, J., Goetze, R., Scholz, S., Seidl, R., and Ernst, A. (2011). Mri scanning in patients implanted with a vibrant soundbridge. *The Laryngoscope*, 121(7):1532–1535.